Effect of different carbon supporter on the Ni/C catalyst for water oxidation

Ke Wang[1], Zhiyan Sun[2], Yan Zhu[1], Li Chunhui[1] ✉

[1]*School of Chemistry and Molecular Engineering, Zhengzhou University, Zhengzhou 450001, People's Republic of China*
[2]*Department of Orthopaedics, the 153rd Central Hospital of PLA, Zhengzhou 450001, People's Republic of China*
✉ *E-mail: lch@zzu.edu.cn*

Published in Micro & Nano Letters; Received on 5th July 2018; Revised on 6th November 2018; Accepted on 12th December 2018

Exploring efficient and inexpensive oxygen evolution reaction (OER) electrocatalysts is essential for clean renewable energy systems. Ni-based nanomaterials have been intensively pursued for NiOOH can play a key role in OER processes in alkaline electrolytes. In this work, Ni nanoparticles (NPs) absorbed onto commercial carbon black and nitrogen-doped reduced graphene oxide as electrochemical catalysts activities in OER have been explored. The study found that the current density and Tafel slope of Ni/C nanocomposite in OER were affected obviously by different carbon supporter and the surface properties of Ni NPs. The work revealed that the Ni NPs electrical contact with supporter and surface hydrophilism of catalytically active species is more important than the size and loaded amount. The awareness of the catalytic kinetics difference deepened their comprehension of the structure–property relationship of the electrocatalyst, which would contribute to the rational design of excellent OER catalysts.

1. Introduction: The increasing environmental problems and energy shortage have initiated a mass of research interest in developing alternative energy storage and conversion systems [1–4]. Hydrogen is a renewable energy carrier because of its high mass-specific energy density (140 MJ/kg) and green combustion products. Compared with traditional hydrogen production from fossil fuels, electrochemical water splitting has been believed high-efficiency, economical and eco-friendly substitute technology to convert electric energy into chemical fuels [5, 6]. Water splitting is composed of two half-cell reactions: the hydrogen evolution reaction and the oxygen evolution reaction (OER), the former can be accomplished at relatively low overpotential but the latter is a sluggish process requiring higher overpotentials because of its high energy-barrier of O–H bond breaking and attendant O–O bond formation [7, 8]. Hence, the overall efficiency of electrolytic water splitting is mainly held back due to the higher anodic overpotential of OER. Precious metal catalysts such as RuO_2 and IrO_2 exhibited high activities but they are too expensive and scarce. In addition, Ir- and Ru-based OER catalysts are unstable in an alkaline environment that is often used in commercial water reaction. The ever-increasing requirement for clean energy brings extensive attention aimed at developing high-active, stable and cheap catalysts for OER under alkaline conditions [9].

In recent years, significant research efforts have been mainly focused on exploring alternatives to find an efficient non-precious and low-cost electrocatalysts in the water splitting such as first-raw transition metallic chalcogen and phosphide, but these materials often have the risks of low stability when functioned as anodes for oxidation in the basic system for the oxidation potential is often more positive than those of the chalcogen and phosphide ions [10]. Thus, transition-metallic oxides or hydroxides which are stable in alkaline solutions are extensively reported for promising electrocatalysts for OER in water splitting. Among these, nickel-based OER nanostructure is one of the most effective oxygen evolution electrocatalysts because of their earth-abundant nature and theoretically high catalytic activity. It is well accepted that NiOOH is the actually catalytically active species during the OER process in basic electrolytes in the common Ni-based catalysts and this can be proved by the anodic oxidation of $Ni^{2+} \rightarrow Ni^{3+}$ in the range of 1.35–1.5 V versus reversible hydrogen electrode (RHE) in linear sweep voltammetry (LSV) curves of Ni-based OER catalysts because it is prior to the onset of oxygen evolution. Therefore, the anions may have a negligible effect on the catalytic activity of Ni-based catalysts and it is necessary to probe the OER catalytic behaviours of metallic Ni NPs and to determine the factors influencing their activities.

In this study, monodisperse metallic Ni NPs of sizes 14 ± 2 nm have been prepared and absorbed onto different carbon supporter, such as N-doped reduced graphene oxide (N-rGO) and XC (Vulcan XC-72, purchased from FuelCellStore, USA). In studying the catalytic properties, it was found that the hydrophilism of Ni NPs surface and the electrical contact between the nanoparticles (NPs) and the supporter were critical in increasing the current density and lowering the Tafel slopes which provided the basis for rational design of better catalysts for OER.

2. Experimental section

2.1. Materials and physical measurements: All the reagents were of analytical grade and were acquired from Sinopharm Chemical Reagent Company, China except for Vulcan XC-72. The crystal structure and phase purity were characterised by using an X'Pert PRO X-ray diffractometer with Cu Kα radiation ($\lambda = 1.5406$ Å) in the 2θ range of 5°–80°. Transmission electron microscopy (TEM) was performed using an FEI Tecnai G2 F20 S-Twin microscope working at an acceleration voltage of 200 kV. X-ray photoelectron spectroscopy (XPS) was performed using a Kratos Axis Ultra DLD X-ray Photoelectron Spectrometer. All the peaks were calibrated with a C 1s spectrum at a binding energy of 284.8 eV.

2.2. Synthesis of Ni NPs: The preparation of Ni NPs is based on the method reported in previous studies [11]. Generally, 1 mmol of nickel(II) acetylacetonate, 2 mmol of 1,2-hexadecanediol, 3 mmol of trioctylphosphine and 40 mmol of oleylamine were mixed and stirred magnetically at 80°C followed by resetting the temperature to 150°C and kept for 20 min. Then the mixture was heated to 200°C for nucleation and growth of Ni NPs. After half an hour, the synthesis was cooled naturally to room temperature. 100 ml of ethanol was added into the black solution and the NPs precipitated overnight followed by washed with ethanol and tetrahydrofuran (THF) three times to remove the surfactant. Then Ni NPs were dispersed in THF for further use.

2.3. Synthesis of the N-rGO: N-rGOs were prepared according to the literature [12]. 10 mg of graphene oxide were sonicated in 35 ml of water to obtain a deep brown solution followed by the addition of 10 mg of urea. Then the solution was transferred into

a 50 ml autoclave and heated at 180°C for 12 h. The system was then allowed to cool to room temperature and the products were deposited at the bottom of the vessel. The final products can be well-dispersed in 20 ml of *N*-methylpyrrolidone (NMP) by sonication.

2.4. Synthesis of Ni/N-rGO: 5 mg of Ni NPs dispersed in 20 ml of THF was added into 20 ml of NMP solution of 10 mg graphene (0.5 mg/ml) and the mixture was sonicated for 1 h. 50 ml ethanol was added and the precipitate was separated from the solvents by centrifuging for 15 min at 4000 rpm and dried under ambient conditions for further use.

2.5. Synthesis of Ni/XC: The method was the same as that of the preparation of the Ni/N-rGO except that XC was used instead of N-rGO. The sample was further treated at 300°C for 30 min and 700°C for 6 h, denoted as Ni/XC-300 and Ni/XC-700, respectively.

2.6. Electrochemical measurement: The OER activities of catalysts were measured by using an electrochemical workstation (CHI 660D, CH Instruments, Austin, TX) in a standard three-electrode electrochemical cell filled with a 0.1 M KOH electrolyte. A glassy carbon (3 mm diameter) coated with a catalyst is the working electrode. A graphite rod and AgCl/Ag electrode were used for the counter and reference electrodes, respectively. The catalysts (about 3.0 mg) and 20 µl of a 5 wt% Nafion solution were dispersed in 2 ml of ethanol and 0.5 ml of deionised water. The resulting mixture was sonicated 20 min to form a homogeneous ink. The catalysts were applied on the surface of the glassy carbon electrode by the dropwise addition of 5 µl of the catalyst ink. All the potentials referred to in this Letter were against RHE without an extra statement. The scan rate for LSV curves was 5 mV s^{-1}. The LSV curves were re-plotted as overpotential (η) versus log current density (log j/[j]) to get Tafel plots for quantification of the OER activities of the investigated catalysts. By fitting the linear portion of the Tafel plots to the Tafel equation ($\eta = b \log j/[j] + a$), the Tafel slope (b) was obtained.

3. Results and discussion: The Ni NPs were characterised by TEM and Fig. 1*b* shows the Ni NPs have a narrow size distribution with an average diameter of 14 ± 2 nm. Based on the (111), (200) and (220) diffraction peaks, the sample can be indexed to pure Ni (JCPDS Card No. 04-0850) with relative weak peaks which are common for nanoscale particles.

For the N-rGO, the high-resolution N 1s XPS spectra can be deconvoluted into three peaks (pyridinic-N, 398.5 eV; graphitic quaternary-N, 400.8 eV; and pyridinic-N^+–O^-, 403.8 eV) according to their bonding energies (Fig. 1*a*), showing graphene oxide was doped by nitrogen atoms successfully.

The TEM images of Ni NPs absorbed onto N-rGO and XC are shown in Figs. 2*a* and *b*. For Ni/XC, the sample was further annealed under a gas mixture of 95% Ar + 5% H_2 for 0.5 h at

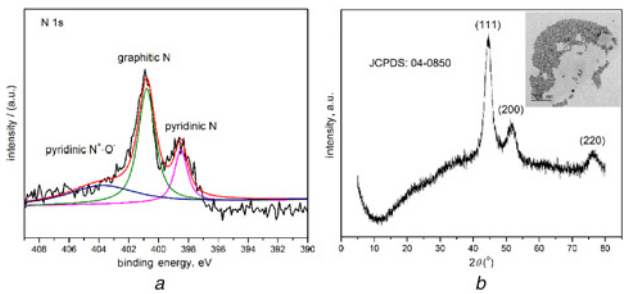

Fig. 1 *XPS of N 1s and XRD pattern of Ni NPs*
a High resolution N 1s spectrum
b X-ray diffraction patterns of Ni NPs. Inset shows its typical TEM images

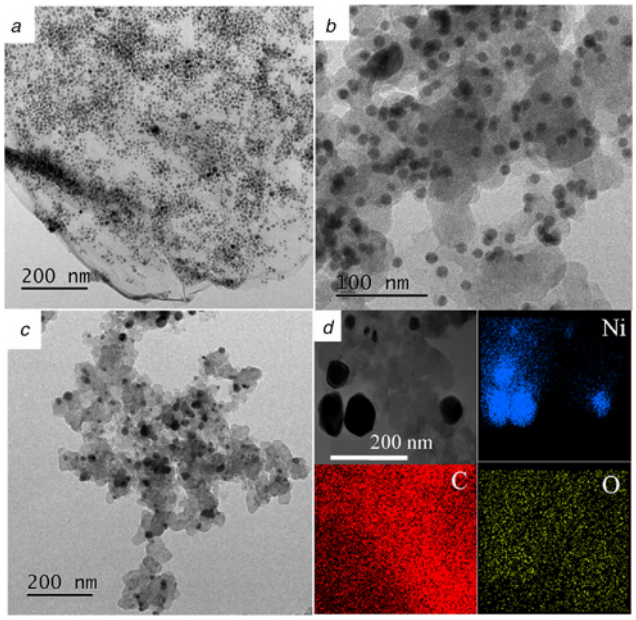

Fig. 2 *TEM images of*
a Ni/N-rGO
b Ni/XC
c Ni/XC-300
d Ni/XC-700 and corresponding elemental maps: Ni (blue), C (red) and O (yellow)

300°C to make Ni NPs in even closer contact with XC and reduce the NPs hydrophobicity. Compared with the un-annealed Ni/XC, the morphologies of Ni/XC annealed at 300°C show obvious change and the sizes of Ni NPs increased from 14 ± 2 to 28 ± 5 nm, the average volumes of Ni NPs quadrupled, as shown in Fig. 2*c*.

Fig. 3*a* shows the iR-corrected LSV curves on the RHE scale. As seen in the LSV curves, there are obvious oxidation peaks of Ni^{2+} to Ni^{3+} between 1.4 and 1.5 V, further illustrating that the valence state of Ni species after each scan was Ni^{2+}, which is easy to comprehend that Ni^{3+} ions are unstable in aqueous solution without an electrical field and are bound to be reduced to Ni^{2+} by surrounding species. Second oxidation waves with an onset potential of ~1.63 V attributed to catalytic water oxidation are also observed, which were consistent with most of the reported Ni-based electrocatalysts. It is noted that the onset potential and current density of Ni/XC-300 are all better than those of Ni/XC although the sizes of Ni NPs of latter are smaller which exposed more surface area to electrolyte, this shows that the sample calcined at 300°C for 30 min did remove the surfactants and increased the catalytic activities [13]. For the same reason, Ni/XC-700 annealed

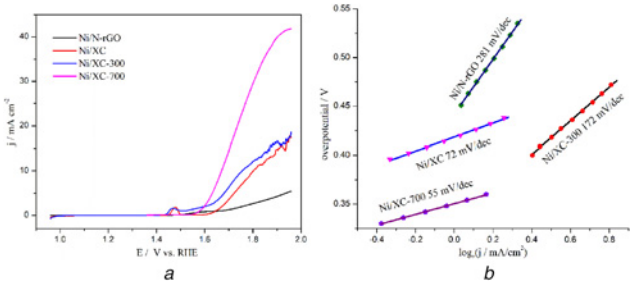

Fig. 3 *LSV curves and Tafel plots of the samples*
a iR-compensated OER polarisation curves
b Corresponding Tafel plots for Ni/N-rGO, Ni/XC, Ni/XC-300 and Ni/XC-700 in 0.1 M KOH

doi: 10.1049/mnl.2018.5367

at 700°C exhibited much better catalytic performance although the aggregation is much more serious, as shown in Figs. 2*d* and 3*a*.

The three samples of Ni NPs loaded on carbon supporter all exhibited obvious OER activities, achieving a current density of 10 mA cm^{-2} at overpotential (η) of 440, 526 and 572 mV for XC supported Ni NPs, respectively. As shown in Fig. 2*d*, the Ni NPs aggregated obviously and the specific area of Ni NPs reduced greatly, which is unfavourable for electrocatalysis. On the other side, the oleylamine absorbed on the Ni NPs surface were removed when annealed and their hydrophilism improved. As for the Ni/N-rGO, the largest current density only reached 5.2 mA cm^{-2} at 1.96 V versus RHE. Note that the largest current density of Ni/XC-700 exceeded 40 mA cm^{-2} at the same overpotential. To clarify the reaction kinetics for the OER electrocatalysis of three samples, Tafel plots (overpotential versus log (j)) derived from polarisation curves for the electrodes were evaluated. Fig. 3*b* shows the Tafel slope of the Ni/N-rGO is 281 mV dec^{-1}, which is much higher than those of the Ni/XC (55, 72 and 172 mV dec^{-1}), implying a more favourable kinetic for the OER of carbon black-supported hybrids.

For these samples, the catalytically active species are all NiOOH and the differences are the supporter and the Ni NPs surface area and hydrophilism. Thus, three factors should be considered to comprehend their difference catalytic activities. First, the electrical conductivity of carbon black is better than that of N-rGO for its oxygen-contained organic groups. Second, compared with two-dimensional N-rGO, carbon black is three-dimensional material and it can provide better electrical contact between the Ni species and supporter. Third, removing capping agents absorbed on nanocrystals to improve the hydrophilism of Ni NPs surface has been widely recognised as a vital route for better electrocatalysts [14, 15]. Theoretically, more electrolytes could be involved in OER for narrower NPs with more surface area, but in fact, it is more difficult to remove hydrophobic capping agents from the narrower NPs surface which will hinder the contact between electrolyte and NPs surface atoms. In the work, Ni NPs were prepared in oleylamine and these NPs are hydrophobic which is unfavourable for the diffusion of species such as OH– during the OER process, so the removal of oleylamine molecules by calcination has a significant impact to their catalytic activities. The comparison of the four samples shows clearly that the hydrophilism of NPs is more important than the sizes of nanocatalysts.

4. Conclusions: In summary, monodisperse Ni NPs of 14 ± 2 nm were successfully prepared and absorbed on different carbon materials such as XC and N-rGO. Electrochemical measurements were used to evaluate the electrocatalytic activity towards the OER and their difference was tentatively discussed. This work showed further confirmed that catalytic performance was affected by three aspects, electrical contact between the catalytically active species and supporter, the electrical conductivity of supporter and hydrophilic nature of catalytically active species, which is helpful for rational design of better catalysts for OER.

5. Acknowledgments: This work was supported by the National Natural Science Foundation of China (grant no. 21271156).

6 References

[1] Pan L., Tang J., Chen Y.H.: 'Synthesis of Fe_3O_4, Fe_2O_3, Ag/Fe_3O_4 and Ag/Fe_2O_3 nanoparticles and their electrocatalytic properties', *Sci. China Mater.*, 2013, **56**, pp. 362–369

[2] Wang G.J., Cheng F., Yu Y., *ET AL.*: 'SC-IrO2NR-carbon hybrid: a catalyst with high electrochemical stability for oxygen reduction', *Sci. China Mater.*, 2013, **56**, pp. 131–136

[3] Wang W.Y., Ma M., Kong M.L., *ET AL.*: 'Cobalt carbonate hydroxide hydrate nanowires array: a three-dimensional catalyst electrode for effective water oxidation', *Micro Nano Lett.*, 2017, **12**, (4), pp. 264–266

[4] Oh S.J., Lee J.H.: 'Preparation and oxidation behavior of cobalt-coated copper powder', *Micro Nano Lett.*, 2017, **12**, (10), pp. 717–721

[5] Stevens M.B., Trang C.D.M., Enman L.J., *ET AL.*: 'Reactive Fe-sites in Ni/Fe (oxy)hydroxide are responsible for exceptional oxygen electrocatalysis activity', *J. Am. Chem. Soc.*, 2017, **139**, pp. 11361–11364

[6] You B., Liu X., Hu G.X., *ET AL.*: 'Universal surface engineering of transition metals for superior electrocatalytic hydrogen evolution in neutral water', *J. Am. Chem. Soc.*, 2017, **139**, pp. 12283–12290

[7] Zhao Y.F., Jia X.D., Chen G.B., *ET AL.*: 'Ultrafine NiO nanosheet stabilized by TiO_2 from monolayer NiTi-LDH precursors: an active water oxidation electrocatalyst', *J. Am. Chem. Soc.*, 2016, **138**, pp. 6517–6524

[8] Tang C., Wang H.F., Wang H.S., *ET AL.*: 'Guest-host modulation of multi-metallic (oxy) hydroxides for superb water oxidation', *J. Mater. Chem. A*, 2016, **4**, pp. 3210–3216

[9] Xi W., Ren Z.Y., Kong L.J., *ET AL.*: 'Dual-valence nickel nanosheets covered with thin carbon as bifunctional electrocatalysts for full water splitting', *J. Mater. Chem. A*, 2016, **4**, pp. 7297–7304

[10] Yeo B.S., Bell A.T.: 'In situ Raman study of nickel oxide and gold-supported nickel oxide catalysts for the electrochemical evolution of oxygen', *J. Phys. Chem. C*, 2012, **116**, pp. 8394–8400

[11] Li M., Chen Y.Z., Ji N., *ET AL.*: 'Preparation of monodisperse Ni nanoparticles and their assembly into 3D nanoparticle superlattices', *Mater. Chem. Phys.*, 2014, **147**, pp. 604–610

[12] Sun L., Wang L., Tian C.G., *ET AL.*: 'Nitrogen-doped graphene with high nitrogen level via a one-step hydrothermal reaction of graphene oxide with urea for superior capacitive energy storage', *RSC Adv.*, 2012, **2**, pp. 4498–4506

[13] Lu S.Q., Zhuang Z.B.: 'Investigating the influence of the adsorbed species on catalytic activity for hydrogen oxidation reaction in alkaline electrolyte', *J. Am. Chem. Soc.*, 2017, **139**, pp. 5156–5163

[14] Zhen Y., Zhou W., Gao Y.J., *ET AL.*: 'Supported Pd–Cu bimetallic nanoparticles that have high activity for the electrochemical oxidation of methanol', *Chem. Eur. J.*, 2012, **18**, pp. 4887–4893

[15] Niu Z. Q., Li Y.D.: 'Removal and utilization of capping agents in nanocatalysis', *Chem. Mater.*, 2014, **26**, pp. 72–83